





A SIMPLE CORRECTION TO THE APPARENT CONDUCTIVITY FROM SURFACE MAGNETIC DIPOLE DATA

Érico Tenório França ^{1,4*}, Cícero Régis ^{1,2},
Luciano Soares da Cunha ³, and Maria Teresa Françoso ⁴

¹Universidade Federal do Pará - UFPA, Graduate Program in Geophysics, Belém, PA, Brazil

²National Institute of Science and Technology of Petroleum Geophysics - INCT, Salvador, BA, Brazil

³Universidade de Brasília - UnB, Geosciences Institute, Campus Darcy Ribeiro, Asa Norte, Brasília, DF, Brazil

⁴Universidade de Campinas - Unicamp, School of Civil Engineering, Architecture and Urban Design, Campinas, SP, Brazil

*Corresponding author email: erico.tenorio@gmail.com

ABSTRACT. A method to improve the determination of apparent conductivities from near-surface electromagnetic dipole data should be simple and easy to implement and use in the field. With this objective, we present a simple correction to the apparent resistivity from surface magnetic dipole data. In contrast with the traditional approach that uses a truncated series to approximate the fields, the proposed method calculates the apparent conductivity by solving a minimization problem using the complete homogeneous half-space analytical solutions for the magnetic field of the dipole sources. In comparison with previous approaches to improve apparent conductivity estimation, this is an extremely simple solution, easily implemented and demanding almost negligible computer time and memory. To illustrate the method, applications to synthetic 2D data and real data are presented. The results show that the method can improve the responses of conductive zones which are difficult to perceive in the raw field data.

Keywords: improved apparent conductivity; conductivity meter; low induction number; Newton's method.

INTRODUCTION

The estimation of apparent conductivities in several geophysical electromagnetic methods that work in the Low Induction Number (LIN) regime is based on approximations of the half-space analytical solutions for the electromagnetic fields from dipolar sources.

Frequency domain responses are commonly given in terms of the mutual coupling ratio Z/Z_0 , where Z is the measured mutual impedance or some field component measured on the surface, and Z_0 is the mutual impedance or field component in free-space. In the cases of magnetic dipoles placed on the surface of a conductive half-space, in the quasi-static regime, there are analytical solutions for the fields measured at the surface. The analytical solutions (Ward and Hohmann, 1987) normalized by the free-space field can be written as power series on the *induction number* θ , which is a function of the source-receiver spacing (offset), frequency, and conductivity of the medium. For low induction numbers the imaginary component of the normalized magnetic field can be approximated as a quadratic function of θ (McNeill, 1980; Méndez-Delgado et al., 1999), which is a linear function of the conductivity. This is the basis for the determination of apparent conductivities in several different survey configurations using magnetic dipole sources. The variants of the Slingram method (e.g., EM31, EM34 and DUALEM-421 systems) determine apparent conductivities in this fashion using only the imaginary

component of the magnetic field (quadrature component) (Spies and Frischknecht, 1987). This linear approach yields a good approximation for the half-space conductivity in the LIN regime, but the approximation quickly degrades as θ grows, which happens in conductive environments.

Alternative methods to determine apparent conductivity have been proposed to overcome some of the limitations of the traditional linear approximation. Hanssens et al. (2019) classify these methods into two approaches: in-phase-quadrature (real and imaginary field components) algorithms, which use all the information from EM fields (Kruk et al., 2000; Huang and Won, 2000; Guillemoteau et al., 2016; He et al., 2017); and quadrature algorithms, which use only the imaginary component of EM fields (Beamish, 2011; Andrade et al., 2016; Hanssens et al., 2019). In the latter approach, all the cited works use the complete solution of Maxwell's equations. Beamish (2011) presented a correction procedure to the LIN apparent conductivity that uses polynomial representations of the measured field in terms of the half-space conductivities. The polynomial coefficients are obtained by least-square fitting of the data. By using the complete solution for a layered model, the method includes the possibility of using the height of the instruments above the surface to improve the approximations. Andrade et al. (2016) obtain the apparent conductivity by minimizing the difference between the observed apparent conductivity and the one calculated from the complete numerical solution, also allowing the source to be positioned at some height from the ground, and using the LIN apparent conductivity as initial guess. Hanssens et al. (2019) introduce the concept of robust apparent electrical conductivity (rECa), which is obtained by interpolation of a value in the apparent conductivity-quadrature curve (ECa-QP), if this curve is monotonic, or using another algorithm (e.g., Huang and Won (2000)) for a non-monotonic curve. In addition, their method assesses the robustness of the rECa estimate, taking into account instrument noise and the effects of subsurface magnetic variation. Non-robust estimates are mainly associated with high induction numbers, which can be caused by environments with high conductivity, high frequencies, and large coil spacings.

The numerical effort to obtain these corrections can be significant because one is forced to implement a calculation using the complete solution to Maxwell's equations, which require the numerical evaluation of improper integrals from the Hankel transform. The otherwise simple process of determining apparent conductivity is complicated by this and other steps, like generating coefficients through least-square fitting of the data and searching in a pre-calculated table, as is done in the method proposed by Beamish (2011).

In practice, all these approaches to improve apparent conductivity from measurements taken in LIN instruments, however complicated they may become, still estimate the conductivity of a homogeneous half-space.

In our view, if the geophysicist is restricted to work with interpretation of apparent conductivities, then the best estimates should be acquired with minimum effort and maximum simplicity in the process. Therefore, our aim in this paper is to offer a very simple correction to improve the estimation of apparent conductivity from magnetic dipole sources using only the currently measured field components in the real world devices.

The method presented here improves the apparent conductivity by using the full analytic expression of the magnetic field of magnetic dipoles on the surface, instead of the low order approximation. It uses an implementation of Newton's method to minimize the single variable function defined as the difference between the analytical half-space solution and the measured field component. It also uses the concept of the cumulative response function presented by McNeill (1980) to calculate a height adjustment for the cases when the sources and receivers may not be considered as located at the surface, again in an extremely simple formulation.

The method takes the measured value, as given by the equipment, as input, and outputs a corrected (or adjusted) value, which we are calling “improved” apparent conductivity. The new apparent conductivity reproduces the true half-space value for a wider range of induction numbers than that for which the linear approach yields reasonably good approximations. This solution is conceptually simple, very easy to implement and extremely computationally inexpensive, while generating values that are compatible with previous approaches within the noise level usually present in the data.

This paper presents only applications to the EM34 configurations (McNeill, 1980), which is a widely used equipment for many applications, but the idea can be implemented for any LIN method in use. The method uses only the imaginary part of the magnetic field, as this is the only information provided by the EM34 equipment, and the results are still in the Low Induction Number range, although that range is extended when compared with the measured data.

To illustrate the method, we show applications to synthetic data from a 2D model, as well as to real data published by Hanssens et al. (2019), and from two surveys performed in Brazil. The results are generated by a single small computer function for each source, and they show that the corrected data are generally closer to the true resistivities than the traditional apparent resistivities (measured data values), especially in the most conductive zones.

This work is intended as a quick and easy way to generate adjusted apparent conductivities that are better for direct interpretation than those provided by the current instruments. It is clear that this is not a substitute for an actual inversion of the data, which must be performed if there is need for a detailed and accurate resistivity mapping of the subsurface. As in previous methods, the application of the functions presented here does not expand the validity of the generated conductivities beyond the LIN regime but, as the examples will show, the adjusted apparent conductivity can improve the interpretation if the user will only work with a first approach directly from the field data.

TRADITIONAL LIN APPARENT CONDUCTIVITY

Apparent conductivity in the low induction number regime is obtained from an approximation for the homogeneous half-space solution of the magnetic field from dipolar sources. The vertical coplanar configuration (VCP) uses the horizontal magnetic component (H_y) generated by a horizontal magnetic dipole, the horizontal coplanar configuration (HCP) and perpendicular configuration (PERP) use the vertical (H_z) and radial (H_r) components generated by a vertical magnetic dipole.

The half-space analytical solutions for these fields (Ward and Hohmann, 1987) are written in terms of the wave number $k = \sqrt{-i\omega\mu_0\sigma}$ in the quasi-static regime and the offset s between transmitter and receiver. The magnetic field components are

$$\frac{H_y}{H_0} = \frac{2}{k^2 s^2} (3 + k^2 s^2 - (3 + 3iks - k^2 s^2)e^{-iks}), \quad (1)$$

$$\frac{H_z}{H_0} = \frac{2}{k^2 s^2} (-9 + (9 + 9iks - 4k^2 s^2 - ik^3 s^3)e^{-iks}), \quad (2)$$

$$\frac{H_r}{H_0} = k^2 s^2 (I_1(iks/2) K_1(iks/2) - I_2(iks/2) K_2(iks/2)), \quad (3)$$

where H_0 is the free space magnetic field in the plane of the dipole, which, for a source with a dipole moment m , is

$$H_0 = -\frac{m}{4\pi s^3}. \quad (4)$$

The solutions for the half-space fields can be written in terms of the induction number θ , defined as

$$\theta = s\sqrt{\frac{\omega\mu_0\sigma}{2}}, \quad (5)$$

where ω represents the angular frequency, μ_0 is the permeability of free space, and σ is the electrical conductivity.

Using the relationship between the wave number and the induction number,

$$iks = (1 + i)\theta, \quad (6)$$

the equations for the field components (Eqs. 1 and 2) become

$$\frac{H_y}{H_0} = \frac{-2}{((i+1)\theta)^2} \left\{ 3 - ((i+1)\theta)^2 - [3 + 3(i+1)\theta + ((i+1)\theta)^2] e^{-(i+1)\theta} \right\}, \quad (7)$$

$$\frac{H_z}{H_0} = \frac{-2}{((i+1)\theta)^2} \left\{ -9 + [9 + 9(i+1)\theta + 4((i+1)\theta)^2 + ((i+1)\theta)^3] e^{-(i+1)\theta} \right\}. \quad (8)$$

Expanding the exponential function into its Taylor power series results in

$$\frac{H_y}{H_0} = \frac{-2}{((i+1)\theta)^2} \left[\frac{-((i+1)\theta)^2}{2} - \frac{((i+1)\theta)^4}{8} + \frac{((i+1)\theta)^5}{24} - \dots \right], \quad (9)$$

$$\frac{H_z}{H_0} = \frac{-2}{((i+1)\theta)^2} \left[\frac{-((i+1)\theta)^2}{2} - \frac{((i+1)\theta)^4}{8} + \frac{5((i+1)\theta)^5}{24} + \dots \right]. \quad (10)$$

The LIN approximation uses only the first two terms, which are the same in both series:

$$\frac{H_z}{H_0} \approx \frac{H_y}{H_0} \approx 1 + i\frac{\theta^2}{2}. \quad (11)$$

Then, the apparent conductivity for both configurations is given by

$$\sigma_a = \frac{4}{\omega\mu_0 s^2} \text{Im} \left\{ \frac{H}{H_0} \right\}, \quad (12)$$

which uses only the imaginary part of the measured field. By performing the same procedure in Equation 3, it is possible to arrive at 12, however, with the negative sign (Spies and Frischknecht, 1987).

The EM34-3 equipment operates in the LIN regime, using three fixed-array settings (offset/frequency) for both the HCP and the VCP (Table 1). The values of frequencies and offsets are chosen so that for a homogeneous half-space all configurations work with the same induction number for the same conductivity. Beamish (2011) presents a list of the main conductivity meters, among them the DUALEM equipment that uses the three configurations of coils.

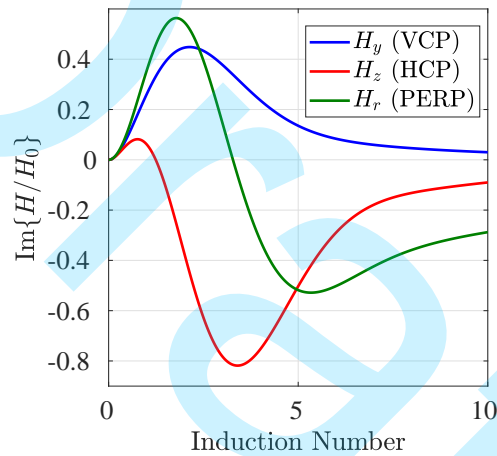
Figure 1 shows the imaginary parts of the half-space fields from the HCP, VCP and the PERP along with the approximate LIN field (Eq. 11), as functions of the induction number. Note that for a given field value the approximation (black line in Fig. 1b) is always at a lesser θ than the smallest of the three possible induction

numbers for all components. Therefore, the apparent conductivity is always less than the true half-space value.

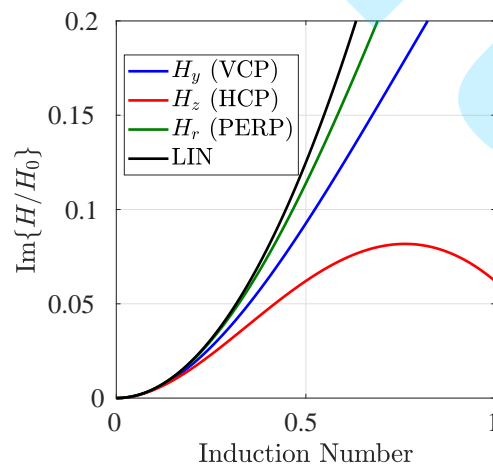
Naturally, the approximation worsens as the induction number increases. When considering the EM34-3 configurations (Table 1), it becomes evident that the relative differences between the approximate and the total half-space fields are already at around 6% for the VCP and 12% for the HCP for $\theta = 0.1$, which is associated with a conductivity of 4 mS/m, or a 250 ohm-m resistivity.

Table 1: EM34-3 arrays offset/frequency and exploration depths.

Offset (m)	Exploration depth (m)		Frequency (Hz)
	VCP (Horizontal dipole)	HCP (Vertical dipole)	
10	7.5	15	6400
20	15	30	1600
40	30	60	400



(a) Dipole fields.



(b) Zoom in to compare with the LIN approximation.

Figure 1: Comparison of the imaginary parts of the full VCP (blue), HCP (red) and PERP (green) fields with the approximate LIN field (black).

IMPROVED APPARENT CONDUCTIVITY

The analytical solution for the field on the surface of a homogeneous half-space is a non linear function of the conductivity of the half-space. The calculation of the apparent conductivity from a measured field component can be formulated as a minimization problem for a function of a single variable. In this case the complete expressions for the homogeneous half-space fields (Eqs. 1, 2 and 3) can be used, and the result is a better approximation for the medium conductivity than those generated by using only one term of the infinite series representing the fields.

Among the several possible approaches to solve this minimization problem, we have chosen to implement Newton's method, because it is conceptually simple, easy to program, and has high convergence rates for the field functions, reaching a solution with the desired precision within few iterations.

Representing the imaginary parts of the normalized magnetic field components by $h_y(\sigma)$, $h_z(\sigma)$ and $h_r(\sigma)$, as functions of the conductivity of the half-space,

$$h_y(\sigma) = \text{Im} \left\{ \frac{H_y}{H_0} \right\}, \quad h_z(\sigma) = \text{Im} \left\{ \frac{H_z}{H_0} \right\}, \quad h_r(\sigma) = \text{Im} \left\{ \frac{H_r}{H_0} \right\}, \quad (13)$$

define the function Φ as the squared difference between h (h_y , h_z or h_r) and the respective measured (observed) field h^o

$$\Phi(\sigma) = \frac{1}{2}(h - h^o)^2. \quad (14)$$

Given a value σ_k , the power series expansion of Φ at $(\sigma_k + \Delta\sigma)$ is

$$\Phi(\sigma_k + \Delta\sigma) = \Phi(\sigma_k) + \Phi'(\sigma_k)\Delta\sigma + \Phi''(\sigma_k)\frac{(\Delta\sigma)^2}{2!} + \Phi'''(\sigma_k)\frac{(\Delta\sigma)^3}{3!} + \dots \quad (15)$$

For small steps $\Delta\sigma$, the function can be approximated by truncating the series at the quadratic term.

$$\Phi(\sigma_k + \Delta\sigma) \approx \Phi(\sigma_k) + \Phi'(\sigma_k)\Delta\sigma + \Phi''(\sigma_k)\frac{(\Delta\sigma)^2}{2}. \quad (16)$$

Then, the step size $\Delta\sigma^*$ needed to reach the minimum, can be determined by finding the point at which the derivative of Φ with respect to $\Delta\sigma$ is zero:

$$\frac{\partial\Phi}{\partial\Delta\sigma} = \Phi'(\sigma_k) + \Phi''(\sigma_k)\Delta\sigma, \quad (17)$$

$$\Delta\sigma^* = -\frac{\Phi'(\sigma_k)}{\Phi''(\sigma_k)}. \quad (18)$$

For a quadratic function of σ , this step would reach the minimum regardless of the value of σ_k . Since Φ is not a quadratic function, this step size is used iteratively:

$$\sigma_{k+1} = \sigma_k - \frac{\Phi'(\sigma_k)}{\Phi''(\sigma_k)}. \quad (19)$$

Each iteration takes a step in the direction of the minimum of the quadratic approximation of the function Φ given by the truncated series (Eq. 16). As the process progresses, the quadratic approximation becomes closer to the function Φ as it approaches its minimum.

The derivatives are

$$\Phi'(\sigma) = \frac{\partial\Phi(\sigma)}{\partial\sigma} = (h - h^o) \frac{\partial h}{\partial\sigma}, \quad (20)$$

$$\Phi''(\sigma) = \frac{\partial^2\Phi(\sigma)}{\partial\sigma^2} = \left(\frac{\partial h}{\partial\sigma}\right)^2 + (h - h^o) \frac{\partial^2 h}{\partial\sigma^2}. \quad (21)$$

The derivatives of h_y , h_z and h_r are calculated analytically from the half-space solutions (Eqs. 1, 2 and 3). To shorten the notation, define the variable t as:

$$t = iks. \quad (22)$$

Then,

$$\frac{\partial h_y}{\partial\sigma} = \text{Im} \left\{ \frac{1}{\sigma t^2} [6 - (6 + 6t + 3t^2 + t^3) e^{-t}] \right\}, \quad (23)$$

$$\frac{\partial^2 h_y}{\partial\sigma^2} = \text{Im} \left\{ \frac{1}{2\sigma^2 t^2} [-24 + (24 + 24t + 12t^2 + 4t^3 + t^4) e^{-t}] \right\}, \quad (24)$$

$$\frac{\partial h_z}{\partial\sigma} = \text{Im} \left\{ \frac{1}{\sigma t^2} [-18 + (18 + 18t + 9t^2 + 3t^3 + t^4) e^{-t}] \right\}, \quad (25)$$

$$\frac{\partial^2 h_z}{\partial\sigma^2} = \text{Im} \left\{ \frac{1}{2\sigma^2 t^2} [72 - (72 + 72t + 36t^2 + 12t^3 + 3t^4 + t^5) e^{-t}] \right\}, \quad (26)$$

and

$$\frac{\partial h_r}{\partial\sigma} = \text{Im} \left\{ \frac{-t^2}{\sigma} \left[2I_1(t/2) K_1(t/2) + I_2(t/2) K_2(t/2) + \frac{t}{2} (I_2(t/2) K_1(t/2) - I_1(t/2) K_2(t/2)) \right] \right\}, \quad (27)$$

$$\frac{\partial^2 h_r}{\partial\sigma^2} = \text{Im} \left\{ \frac{-t^2}{4\sigma^2} \left[(8 + t^2)(I_1(t/2) K_1(t/2) - I_2(t/2) K_2(t/2)) + t (I_2(t/2) K_1(t/2) - I_1(t/2) K_2(t/2)) \right] \right\}. \quad (28)$$

This inverse problem is ill-posed because there are two induction numbers associated with a given field measurement. To cope with this difficulty, the process simply uses the apparent conductivity given by the LIN approximation as the first guess to start the process. Using it ensures that the reached minimum of Φ always will be at the lowest half-space conductivity compatible with the measured field because its induction number is always a point for which the function has positive derivative. Therefore, this approach is still a LIN method.

The iterations stop when there is no significant variation in the conductivity. The result is the true value of the homogeneous half-space conductivity with the desired precision used as the stopping criterium.

Figure 2 illustrates the comparative analysis between the apparent conductivity obtained from the EM34 equipment and the improved conductivity for a homogeneous half-space. In the PERP case, the DUALEM-4 equipment configuration is employed with a 4 m offset and a frequency of 9000 Hz. For all settings, the true half-space value is achieved for the low range of induction numbers up to the value where the curves in Figure 1 reach their maxima.

When applied to a measured value of apparent conductivity the algorithm works as illustrated in Figure 3:

First, the magnetic component $\text{Im}\{H/H_0\}$ (H_y , H_z or H_r) is calculated from the observed apparent conductivity through Equation 12 (vertical arrow up); Then, this value is found in the corresponding magnetic field function (either Eqs. 1, 2 or 3) by the minimization of the function defined by Equation 14 (horizontal arrow); Finally, the minimum gives the adjusted apparent conductivity (vertical arrow down).

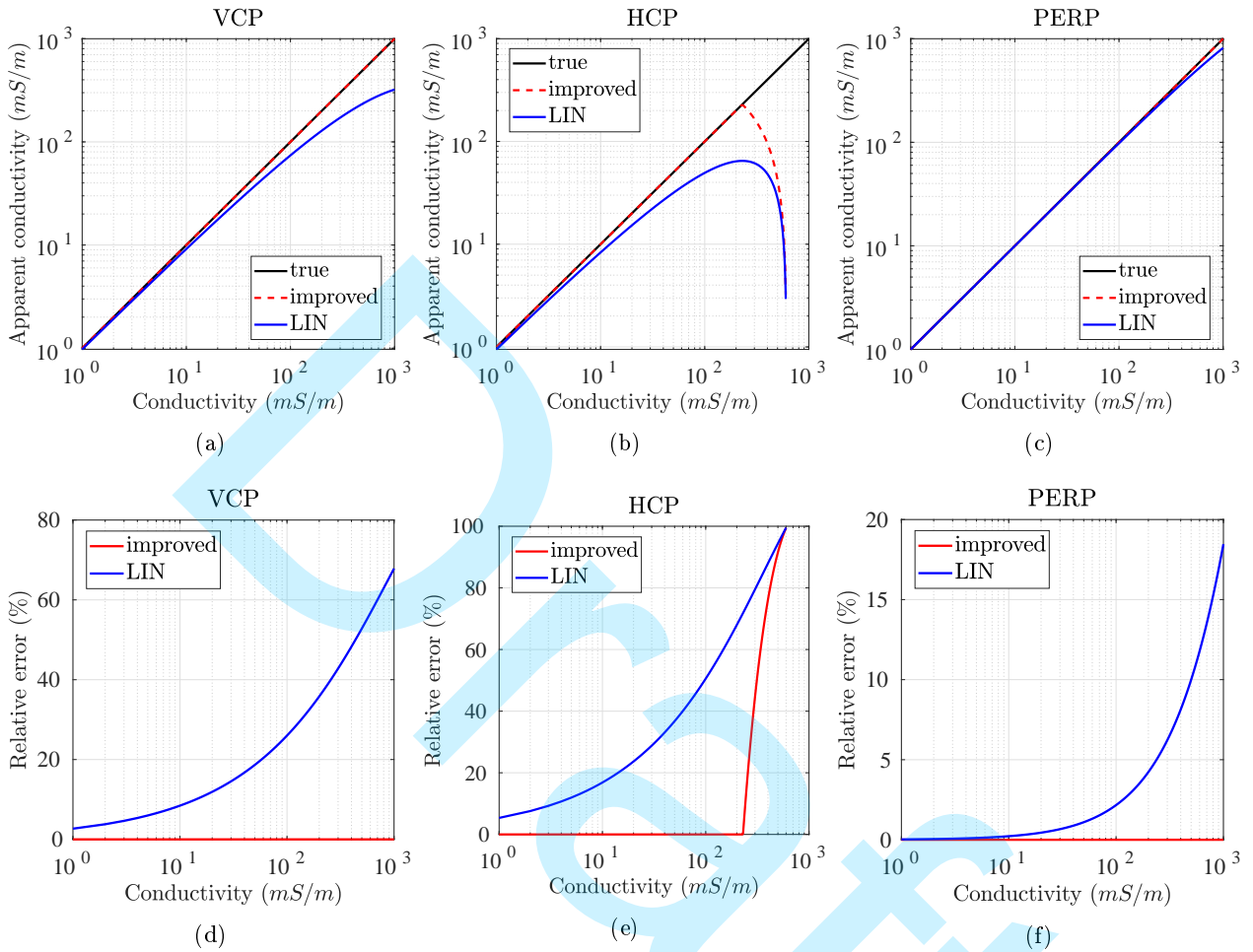


Figure 2: Comparison of improved and EM34 apparent conductivities for VCP (a), HCP (b), and PERP (c) data from a homogeneous half-space. The corresponding relative errors are shown in (d), (e), and (f).

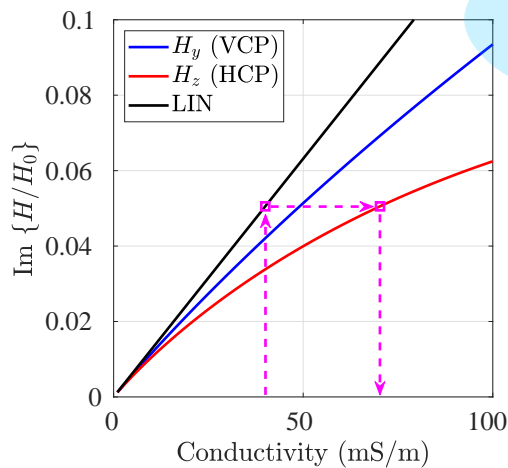


Figure 3: Illustration of the variation found in the apparent conductivity from the measured to the adjusted value.

The gain in the conductivity estimation is represented by the horizontal arrow in Figure 3. This variation will be small for the smallest induction numbers but will grow as θ grows in the valid intervals of each function. The final apparent conductivity is always higher than the original equipment reading.

HEIGHT CORRECTION

The calculation of apparent conductivity using the LIN approximation is done by taking the magnetic dipoles located on the ground surface. However, in most real cases the measurements taken by conductivity meters are made at a certain height from the ground. The works by [Beamish \(2011\)](#), [Andrade et al. \(2016\)](#) and [Hanssens et al. \(2019\)](#) show that the height effect generates underestimated apparent conductivity values. We present a height correction procedure that uses the cumulative response function presented by [McNeill \(1980\)](#).

In a two layer model, the apparent conductivity given by [McNeill \(1980\)](#) is

$$\sigma_a = \sigma_1 [1 - R_{V,H,P}(z_1)] + \sigma_2 R_{V,H,P}(z_1), \quad (29)$$

where σ_1 and σ_2 are the conductivities of the top and bottom layers (mS/m), and z_1 is the ratio between the thickness of the first layer (h_1) and the offset (s). The cumulative response functions $R_{V,H,P}(z_1)$ for the VCP, HCP, and PERP configurations are, respectively,

$$R_V(z_1) = (4z_1^2 + 1)^{1/2} - 2z_1, \quad (30)$$

$$R_H(z_1) = \frac{1}{(4z_1^2 + 1)^{1/2}}, \quad (31)$$

$$R_P(z_1) = 1 - \frac{2z_1}{(4z_1^2 + 1)^{1/2}}. \quad (32)$$

Our approach considers the height of the dipole above ground as the thickness of the first layer (Fig. 4) in a two layers model, with the air conductivity equal to zero. The apparent conductivity given by Equation 29 then becomes

$$\sigma_a = \sigma_2 R_{V,H,P}(z_1). \quad (33)$$

Therefore, the Height Corrected (HC) apparent conductivity is given by

$$\sigma_a^{HC} = \frac{\sigma_a}{R_{V,H,P}(z_1)}. \quad (34)$$

In this procedure, the height correction is first applied to the LIN apparent conductivity (conductivity meter measurements) and then the new estimation (improved data) is generated using Newton's method.

The height correction is needed in the cases when the coils are carried at some height. However, even in the more common situation for an EM34 survey, which is performed with the loops touching the ground, this correction is useful, as the examples will demonstrate. In this case, in the horizontal coplanar configuration, the coils are laid horizontally on the ground, which makes any height correction unnecessary, whereas in the vertical coplanar configuration the coils are placed vertically and their centers are located above ground, so the dipole location is at a height equal to the coil radius. Therefore, even in traditional surveys, a height correction

may improve the VCP data.

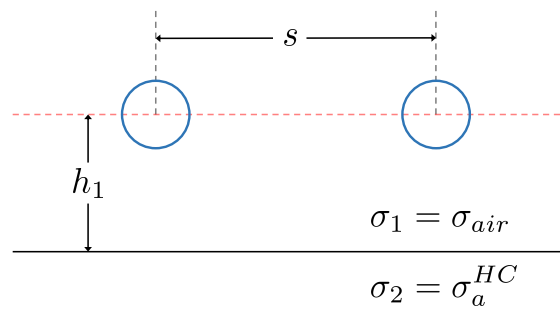


Figure 4: Model with vertical coplanar loops located above the ground surface.

Figure 5 shows relative error maps of apparent conductivity, varying the transmitter-receiver height, and the half-space true conductivity. The map for each coil configuration, in which the EM34 arrangement is used for the VCP (offset 10 m), and for the HCP and PERP the DUALEM arrangement is used (offset 1 m). The top map shows the errors in the data without any height correction. Then, the improved apparent conductivity is shown without height correction (middle) and with height correction (bottom). The height correction together with the apparent conductivity improvement procedure reached the lowest values of relative errors, with maximum values of 21% (VCP and HCP) and 7% (PERP). Therefore, the height correction proves to be effective for a wide range of ground conductivity values, for height values up to 1 m.

Especially significant are the values at height around 0.5 m because this is usually the radius of the EM34 coils, so that even in a traditional survey the improved values with height correction may be significantly better than those given by the equipment, particularly for the most conductive soils, for which the error may decrease from over 70% to about 10%.

IMPLEMENTATION DETAILS

Appendix A contains three MATLAB functions (called `Newton_VCP`, `Newton_HCP` and `Newton_PERP`) designed to generate the improved apparent conductivity value for a single measurement of an conductivity meter survey. The inputs are the apparent conductivity, as given by the conductivity meter (e.g., EM34 or DUALEM), the frequency, and the offset and height of the transmitter-receiver pair.

The main stopping criterium is the value of the relative difference between the quadrature component of the magnetic field in two consecutive iterations. The minimum acceptable difference is stored in the variable `tol`, which, in this implementation is set to 0.01, meaning that the process will stop at a variation of less than 0.01%.

If the measured data falls outside the range of the admissible magnetic field quadrature component, in which case the instrument returns a negative value, the functions will return the same value as the input.

If the quadrature component is close to one of the peaks of the curves in Figure 1a, the minimum of the adjusting function Φ (Eq. 14) is located in the bottom of a wide valley, in a region of very low derivative around the minimum. In this case, the second derivative of Φ around the minimum is close to zero, and it is possible that the step given by Equation 19 overshoots the minimum. To cope with this possibility, whenever the new Φ is larger than the previous value, the functions cut the calculated step in half until convergence is achieved

or the number of cuts is greater than 4, in which case the function returns the last calculated conductivity.

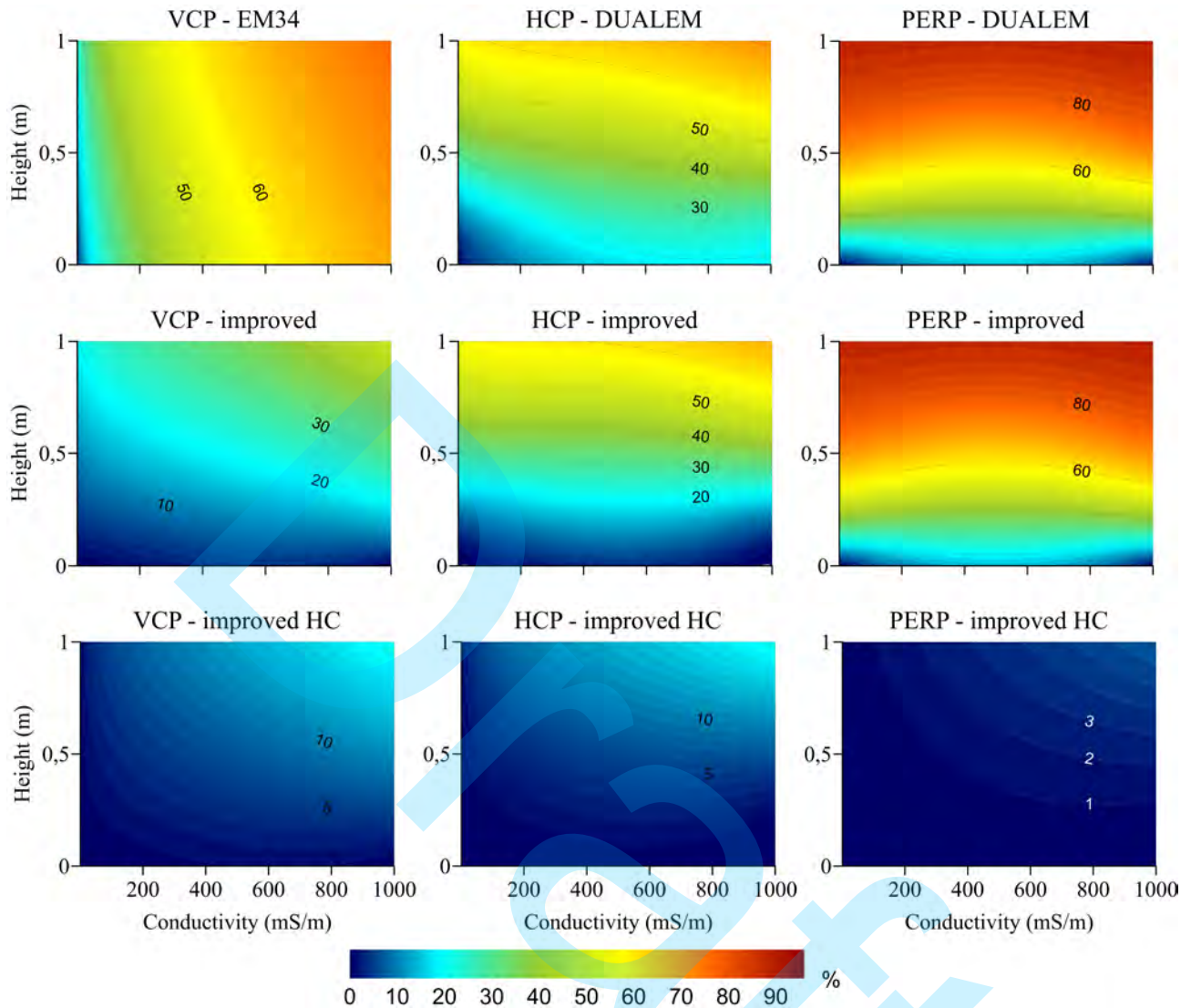


Figure 5: Relative error maps of apparent conductivity as function of the height from the ground and the true conductivity of the half-space. Top: original data; Middle: improved apparent conductivity; Bottom: improved apparent conductivity with height correction.

Noise in the data may result in a measurement of the imaginary component of the magnetic field that is above the maximum possible value for a homogeneous half-space. In this case, the process simply returns the maximum value by the process described in the previous paragraph. In any other instance, noise in the data is directly transferred to the calculated apparent conductivity, and the user must exercise the same level of caution, regarding noise, as when using the unaltered, original data.

APPLICATION TO SYNTHETIC DATA

The synthetic H_z and H_y data were generated with a nodal finite element code, using a non-structured mesh. The finite element method is implemented as described in Jin (2015), using a 2.5D formulation in which the geometry of the 3D electromagnetic field in the 2D medium is transformed by the application of the Fourier Transform to the coordinate that defines the strike direction, as described by Li and Key (2007). The field is

written as the sum of two parts: the so called *primary* field, which is the one generated by the source in the background 1D layered model, and the *secondary* field, which is a perturbation defined as the difference between the total field in the 2D model and the primary one. Then, the differential equations are written in terms of the secondary electric and magnetic components in the strike direction, using homogeneous Dirichlet conditions at boundaries located far enough from the 2D heterogeneities.

The model simulates a geoelectrical environment with a 5 m thick top layer with a 20 mS/m conductivity over a conductive (100 mS/m) infinite basement and a trough-shaped feature with the same resistivity as the upper layer (Fig. 6). These conductivities were chosen to be far from the low values for which the LIN approximation yields the best results. The survey line is 200 m long, with 5 m spacing between measurements, and 0.5 m height of the transmitter-receiver for the VCP.

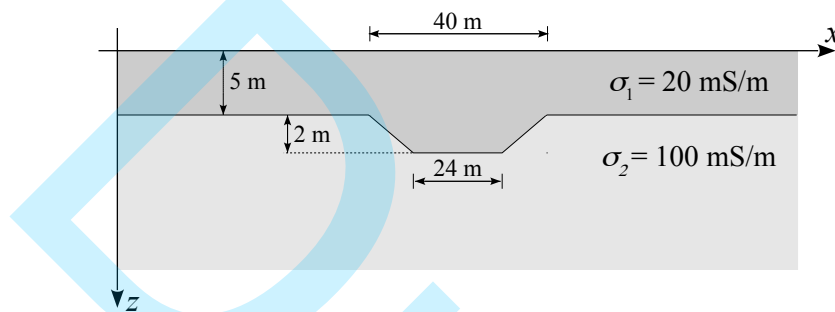


Figure 6: 2D geoelectrical model used in apparent conductivity sections.

The results are presented as apparent conductivity sections, using the “exploration depths” specified in the EM34 technical notes (Table 1). The thickness of the top layer (5 m) is less than the lowest specified EM34 exploration depth, which is 7.5 m for the VCP 10 m offset configuration. This top layer is enough to perturb the field in the otherwise homogeneous earth and hinder the LIN half-space approximation. The 2D structure at the base of the layer further distorts the fields at the surface in the central regions of the survey line, especially the VCP data.

Figure 7 shows the apparent conductivity sections. The influence of the top layer is felt over all frequencies in both VCP and HCP configurations. The apparent conductivities in the corrected sections are consistently closer to the true values than those in the unchanged EM34 sections. The corrected values reflect the true conductivity of the basement in both the VCP and HCP configurations.

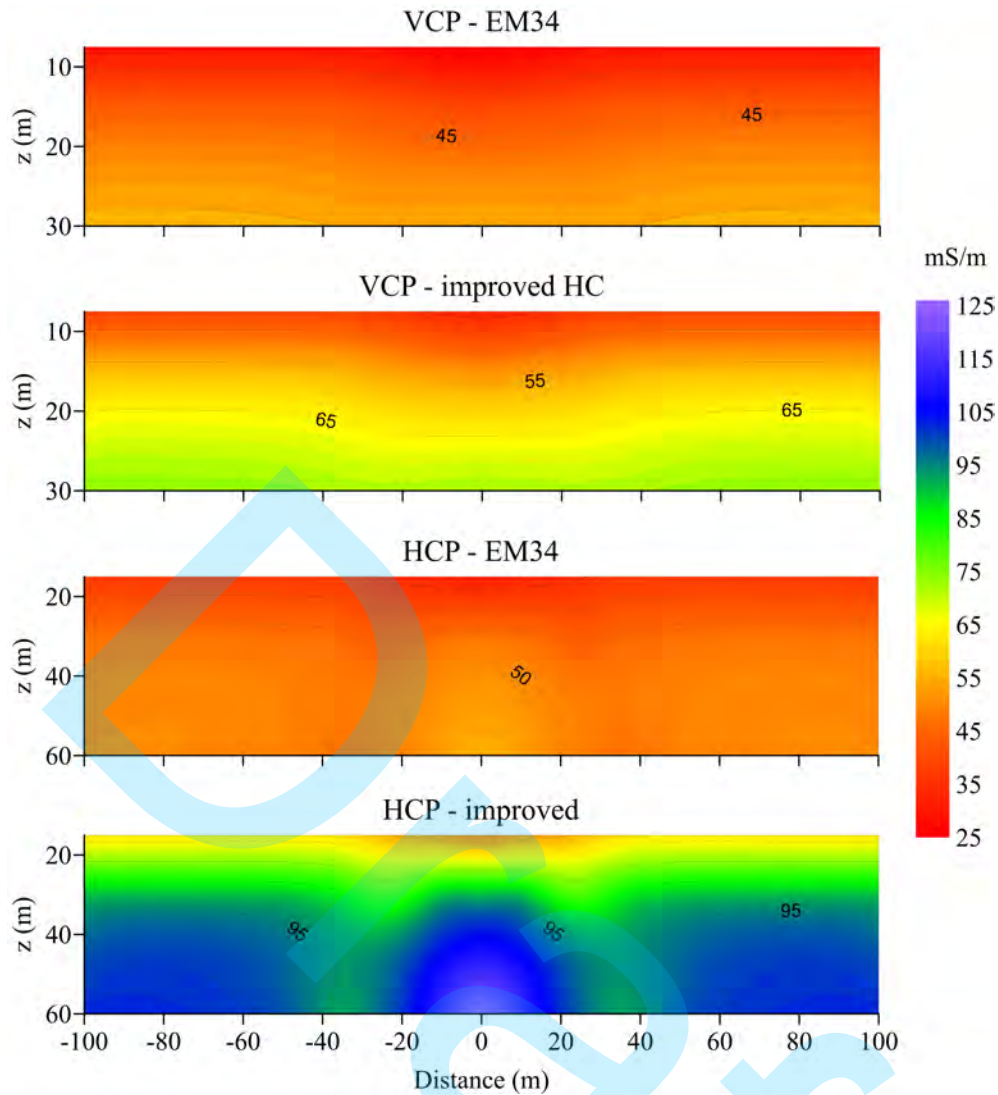


Figure 7: Comparison between the improved and the LIN apparent conductivity for the synthetic data generated by the model in Figure 6. Height correction for the improved VCP section ($h_1 = 0.5$ m).

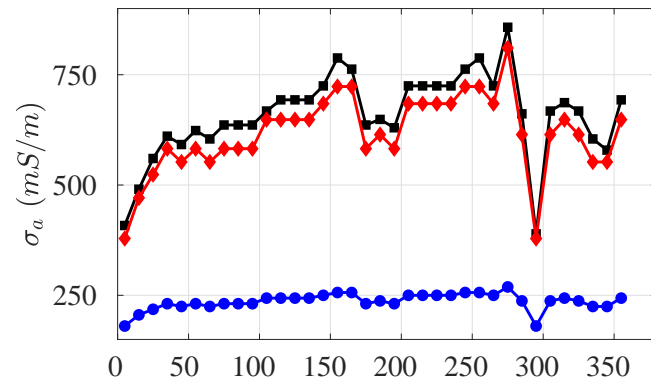
APPLICATION TO REAL DATA

Hanssens et al. (2019) real data

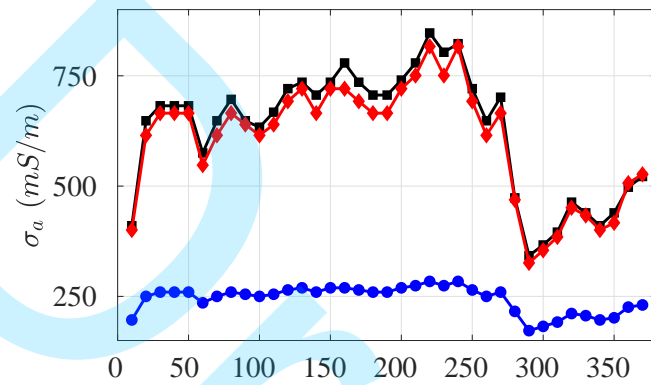
This data set is from an EM34-3XL survey published by Hanssens et al. (2019). The data was acquired using the 3 offsets of the VCP configuration only. The measurements were taken every 10 m, and the transmitter and receiver coils have their centers located at the height of the radius (0.515 m and 0.345 m, respectively). The profiles were obtained in an intertidal zone of a beach during low tide, that is, a high salinity environment. Figure 8 shows the EM34-3XL data, for the 3 offset-frequency arrays.

Hanssens et al. (2019) show that the EM34-3XL apparent conductivities are, as expected, strongly underestimated relative to the concept of the robust apparent electrical conductivity (rECa) introduced by them. After digitizing these data, we have applied our height correction ($h_1 = 0.5$ m) and then calculated the improved apparent conductivity. The results are compared with the original data in Figure 8.

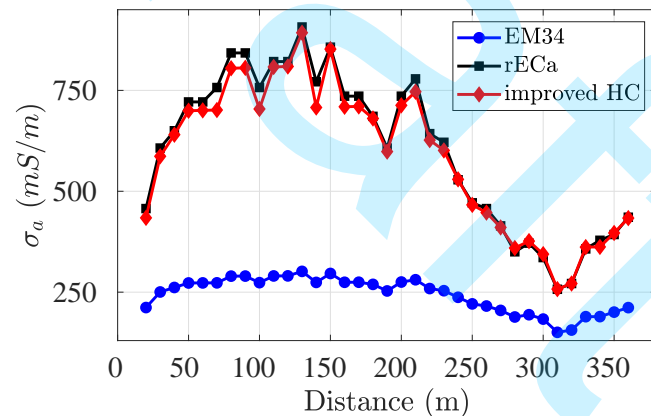
The values generated by our simple method are very close to those of the rECa, which are generated using the complete solution of Maxwell's equations for layered models. The differences decrease with the increase of



(a) VCP data, 10 m offset.



(b) VCP data, 20 m offset.



(c) VCP data, 40 m offset.

Figure 8: Comparison between the apparent conductivity values of the EM34-3XL, rECa, and improved apparent conductivity with height correction ($h_1 = 0.5$ m), for the data presented by [Hanssens et al. \(2019\)](#).

the transmitter-receiver offset, mainly because the height effect is relatively smaller for the greater offsets.

First field example

The following data were acquired in the city of Salinópolis, state of Pará, Brazil. The local geology consists of a miocene carbonate sequence (Pirabas Formation), which is covered by more resistive continental tertiary and quaternary terrigenous sediments (Barreiras e Post-Barreiras) ([Rossetti, 2001](#)). The Pirabas Formation is the

main source of local groundwater supply.

The measurements were taken in the vicinity of a ground water well for which there are logging data available. The EM34 data set is composed of 20 measurements acquired every 10 m with the two coplanar configurations, northeast-southwest direction as shown in the Figure 9.

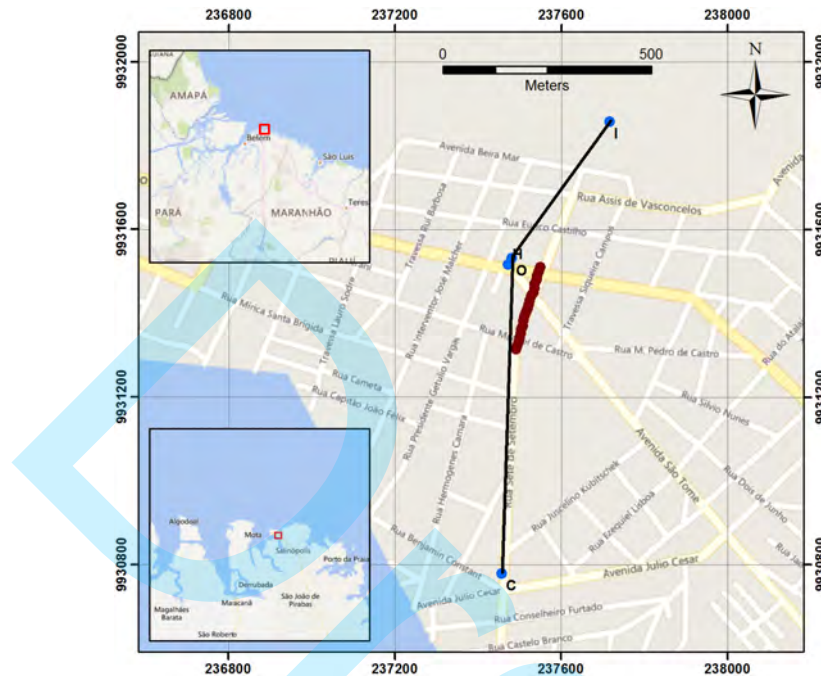


Figure 9: Location of the city of Salinópolis, and location of the lithological section **C-H-I** proposed by [Freimann et al. \(2014\)](#) in black line, the blue points being the wells **C**, **H**, **I** and **O**. The red dots are the EM34 observations taken in the northeast-southwest direction.

Figure 10 shows the apparent conductivity sections built with the original EM34 data and the corrected data. Height correction ($h_1 = 0.5$ m) was only applied for improved VCP section. There are notable differences between the two VCP sections, mainly in the final portion of the profile, where there is a conductive region whose difference between the sections is practically 10 mS/m. The most remarkable result is found in the improved HCP data section, which reveals a more conductive deep region (≈ 90 mS/m), whereas the corresponding EM34 section reaches a maximum conductivity of approximately 45 mS/m. Furthermore, the improved VCP and HCP sections show a correlation that can be noted at the 45 mS/m isovalue line.

[Freimann et al. \(2014, in portuguese\)](#) presented the lithological section reproduced in Figure 11, based on the interpolation of well logging data. Their interpretation indicates that there are two deep aquifers located around the depths of 70 e 105 m below sea level (0 in the vertical scale). These conductive layers exert influence on the measured magnetic fields, but have remained almost undetected in the conventional sections. In the adjusted sections, however, the deepest zone in the HCP data shows a very distinguished conductive zone, indicating that these data are in the highest of the low induction number range, so that the gain illustrated in Figure 3 is highest.

An interpretation based on the adjusted sections will be more likely to infer the conductive aquifers than one based on the original data.

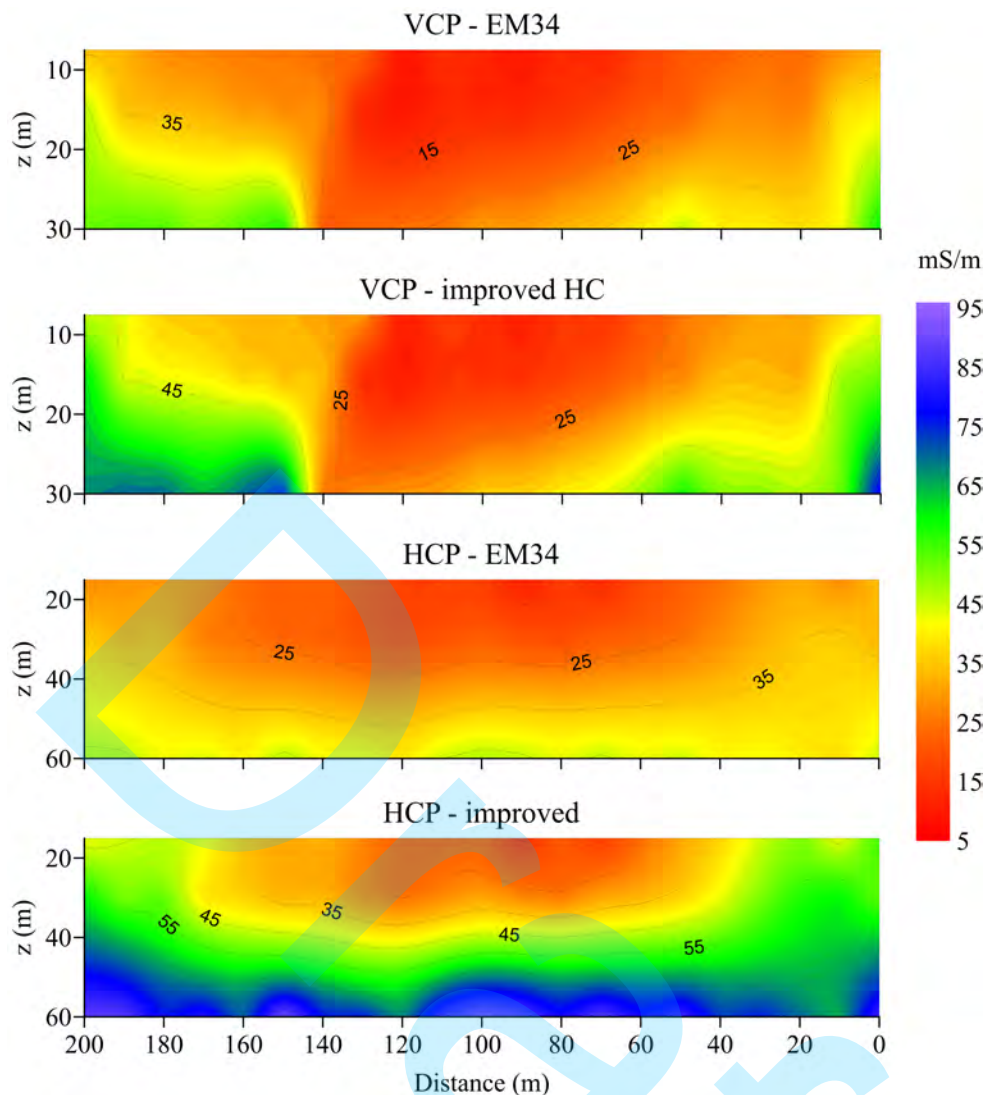


Figure 10: Comparison between the improved and the traditional LIN apparent conductivity for the real data. Height correction for the improved VCP section ($h_1 = 0.5$ m).

Second field example

The second area of study is in the municipality of Beberibe, Ceará State, Brazil. Three distinct hydrogeological domains exist in this region: crystalline rocks, sedimentary cover and alluvial deposits. In the domain of crystalline rocks, the occurrence of groundwater is conditioned by a secondary porosity represented by fractures and cracks, which translates into randomly distributed discontinuous small reservoirs. The sedimentary domain includes the Barreiras Formation sediments and is characterized by a significant faciological variation, with intercalations of more and less permeable levels. In alluvial deposits, there are recent sand-clay sediments, with high permeability, which, despite their small thicknesses, produce significant water flows.

The EM34 survey was conducted at the location presented in Figure 12. The measurement spacing was 40 m. A Vertical Electrical Sounding (VES) was performed at the position indicated by the red triangle using the Schlumberger array, with current electrode apertures ($AB/2$) ranging from 1.5 to 150 m, oriented in the north-south direction.

Figure 13 shows the apparent conductivity sections. Again, height correction ($h_1 = 0.5$ m) was only applied

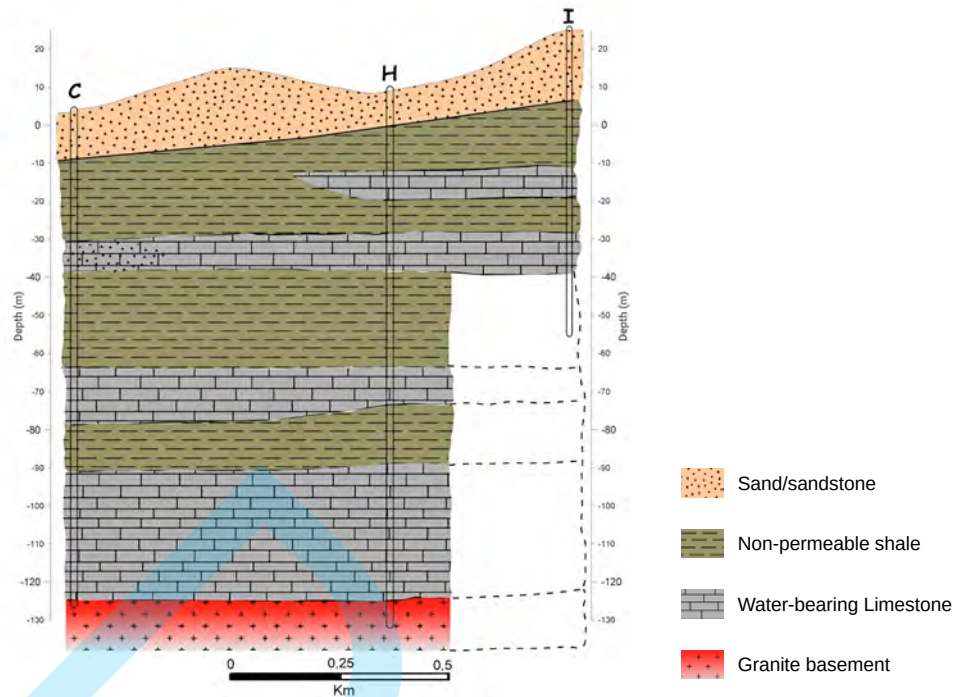


Figure 11: Lithological section **C-H-I** presented by [Freimann et al. \(2014\)](#).

for improved VCP section. The biggest differences between the two sets of data are again seen in the HCP section, which is sensitive to greater depths. The top of a conductive layer, between the depths of 20 and 30 meters, is much more clearly seen in the corrected section than in the original data.



Figure 12: Location of the EM34 measurements and the Vertical Electrical Sounding (VES) point (red triangle). The measurements followed the east-west orientation.

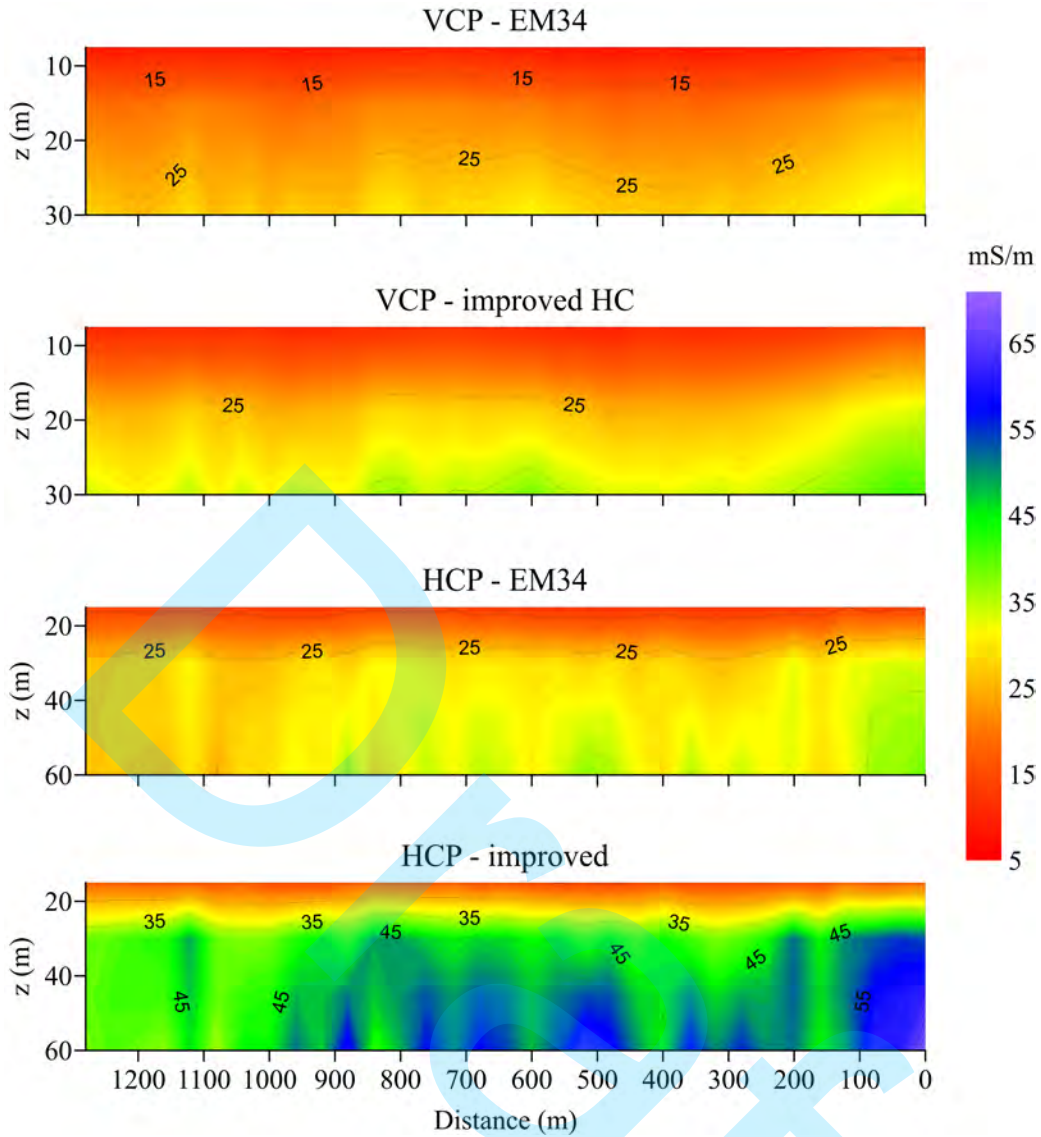


Figure 13: Comparison between the improved and the traditional LIN apparent conductivity for the Beberibe data. Height correction for the improved VCP section ($h_1 = 0.5$ m).

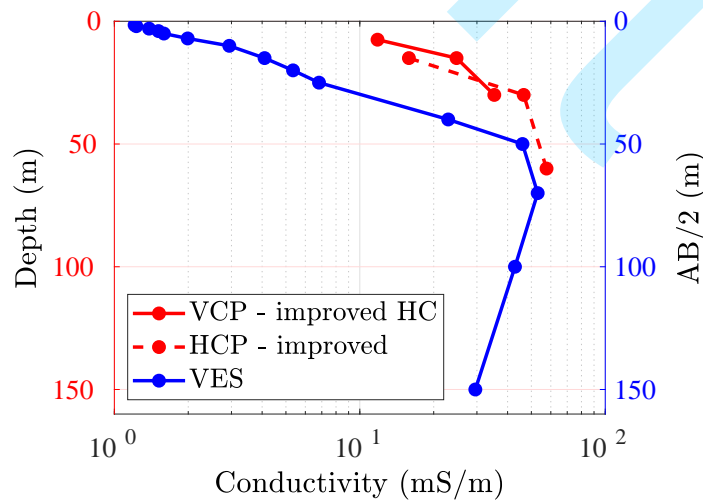


Figure 14: Comparison between the improved apparent conductivity (VCP and HCP) and the VES apparent conductivity, at the measurement position 680m (red trigonle) from sections in Figure 13.

For comparison, Figure 14 shows the VES data gathered in the position 680 m, as shown in Figure 12 (red triangle). The VES apparent conductivity, like that of our adjusted EM34 data, is calculated to correspond to the true value if the measurements were performed over a homogeneous half-space. Therefore, the VES data are in better agreement with the adjusted data than with the original EM34 measurements, with a maximum conductivity between 50 and 60 mS/m.

CONCLUSIONS

We have presented a method to determine apparent conductivities from electromagnetic dipole data that uses a minimization code to estimate conductivity from the complete homogeneous half-space solutions for the magnetic field, instead of using the traditional truncated power series. The method takes the usual measurements as input and generates adjusted apparent conductivities with negligible computational cost.

The proposed method generates apparent conductivities that converge to the traditional EM34 data in the most resistive environments, but that differ from the conventional data in conductive zones for which the conductivities estimated by the low order approximation are lower than the true values in the geological environments.

The presented Matlab functions can be easily translated to any computer programming language, and the code can be run in any portable computer.

Although this process is not a substitute for an inversion work, it is capable of improving the estimation of apparent conductivities without adding any significant time. It can be applied in the field immediately after the EM34 data are gathered.

In comparison with all previous approaches to improve the estimation of apparent conductivities, this method has three practical advantages:

- It is conceptually simpler – It simply finds the conductivity value in the complete half-space analytical solution, rather than using only one term in an infinite series, and performs a height correction by few elementary arithmetic operations.
- It is easier to implement – The half-space solutions and all their derivatives are calculated analytically and the only part of the expressions that is not simple arithmetic is the exponential function. The translation from the Matlab code shown in the appendix to any programming language is straightforward.
- It is computationally cheaper: Even though modern computers can run even the more complex approaches in very short times, the number of operations and the memory requirement necessary to generate the improved apparent conductivity in this method is considerably smaller than in alternative approaches because it avoids the calculation of improper integrals and other tasks like searching on pre-calculating tables.

In our view, if the geophysicist needs to gather the maximum amount of information from the data, then the greatest returns will come from performing inversion, rather than interpreting apparent conductivities. However, in many cases all that is available are apparent conductivities. For these situations, from a practical perspective, we submit that any complexity beyond the level implemented in our method is unnecessary in view of the small gain for the effort.

DATA AVAILABILITY

The data that support the findings of this study, as well as Matlab and Fortran codes for the correction functions, are available from the corresponding author.

APPENDIX A: MATLAB FUNCTIONS

Vertical coplanar configuration

```
function San = Newton_VCP(sa, r, f, h0)
%
% Calculates the improved apparent conductivity from conductivity meter data,
% using Newton's method.
% Inputs:
% sa => apparent conductivity (mS/m);
% r => transmitter-receiver offset (m);
% f => frequency (Hz);
% h0 => height (m).
% Output:
% San => improved apparent conductivity (mS/m)
%
Rv = sqrt(4*(h0/r)^2 + 1) - 2*h0/r;
sa = sa / (1000 * Rv);
ho = sa * (2.e-7 * pi*pi * r^2 * f);
t = (1+1i)* r * sqrt(sa*f/10) * 2e-3 * pi;
h = -2 * ( 3 -t^2 - ( 3 + 3*t + t^2 )*exp(-t) )/(t^2);
fi0 = (imag(h)-ho)^2;
s0 = sa;
San = sa;
tol = 0.01;
cont1 = 0;
while ( 100*abs(ho-imag(h))/ho > tol )
    cont1 = cont1 + 1;
    dHds = imag( 6/t^2 - (6/t^2 + 6/t + 3 + t)*exp(-t) ) / San;
    d2Hds2 = imag((-24+(24+24*t+12*t^2+4*t^3+t^4)*exp(-t))/(2*San^2*t^2));
    ds = dHds * (imag(h)-ho) / ( dHds^2 + (imag(h)-ho)*d2Hds2 );
    San = s0 - ds;
    t = (1+1i)* r * sqrt(San*f/10) * 2e-3 * pi;
    h = -2 * ( 3 -t^2 - ( 3 + 3*t + t^2 )*exp(-t) )/(t.^2);
    fi = (imag(h)-ho)^2;
    cont2 = 0;
    while (fi>fi0)
        cont2 = cont2 + 1;
        San = s0 - ds/2;
        t = (1+1i)* r * sqrt(San*f/10) * 2e-3 * pi;
        h = -2 * ( 3 -t^2 - ( 3 + 3*t + t^2 )*exp(-t) )/(t.^2);
        fi = (imag(h)-ho)^2;
        if cont2 > 4
            break
        end
    end
    fi0 = fi;
    s0 = San;
    if cont1 > 9
        break
    end
end
San = San * 1000;
```

Horizontal coplanar configuration

```

function San = Newton_HCP(sa, r, f, h0)
%
% Calculates the improved apparent conductivity from conductivity meter data,
% using Newton's method.
% Inputs:
%   sa  => apparent conductivity (mS/m);
%   r   => transmitter-receiver offset (m);
%   f   => frequency (Hz);
%   h0  => height (m).
% Output:
%   San => improved apparent conductivity (mS/m)
%
Rh = 1 / sqrt(4*(h0/r)^2 + 1);
sa = sa / (1000 * Rh);
ho = sa * (2.e-7 * pi*pi * r^2 * f);
t = (1+1i)* r * sqrt(sa*f/10) * 2e-3 * pi;
h = -2 * ( -9 + ( 9 + 9*t + 4*t^2 + t^3)*exp(-t) )/(t^2);
fi0 = (imag(h)-ho)^2;
s0 = sa;
San = sa;
tol = 0.01;
cont1 = 0;
while ( 100*abs(ho-imag(h))/ho > tol )
    cont1 = cont1 + 1;
    dHds = imag((-18+(18+18*t+9*t^2+3*t^3+t^4)*exp(-t))/(San*t^2));
    d2Hds2 = imag((72-(72+72*t+36*t^2+12*t^3+3*t^4+t^5)*exp(-t))/(2*(San*t)^2));
    ds = dHds * (imag(h)-ho) / ( dHds^2 + (imag(h)-ho)*d2Hds2 );
    San = s0 - ds;
    t = (1+1i)* r * sqrt(San*f/10) * 2e-3 * pi;
    h = -2 * ( -9 + ( 9 + 9*t + 4*t^2 + t^3)*exp(-t) )/(t^2);
    fi = (imag(h)-ho)^2;
    cont2 = 0;
    while (fi>fi0)
        cont2 = cont2 + 1;
        San = s0 - ds/2;
        t = (1+1i)* r * sqrt(San*f/10) * 2e-3 * pi;
        h = -2 * ( -9 + ( 9 + 9*t + 4*t^2 + t^3)*exp(-t) )/(t^2);
        fi = (imag(h)-ho)^2;
        if cont2 > 4
            break
        end
    end
    fi0 = fi;
    s0 = San;
    if cont1 > 9
        break
    end
end
San = San * 1000;

```

Perpendicular configuration

```

function San = Newton_PERP(sa, r, f, h0)
%
% Calculates the improved apparent conductivity from conductivity meter data,
% using Newton's method.
% Inputs:
%   sa  => apparent conductivity (mS/m);
%   r   => transmitter-receiver offset (m);
%   f   => frequency (Hz);
%   h0  => height (m).
% Output:

```

```

% San => improved apparent conductivity (mS/m)
%
Rp = 1 - 2*h0/(r*sqrt(4*(h0/r)^2 + 1));
sa = sa / (1000 * Rp);
ho = sa * (2.e-7 * pi*pi * r^2 * f);
t = (1+1i)* r * sqrt(sa*f/10) * 2e-3 * pi;
h = t^2*(besseli(1,t/2)*besselk(1,t/2) - besseli(2,t/2)*besselk(2,t/2));
fi0 = (imag(h)-ho)^2;
s0 = sa;
San = sa;
tol = 0.01;
cont1 = 0;
while ( 100*abs(ho-imag(h))/ho > tol )
    cont1 = cont1 + 1;
    dHds = imag(t^2*( 2*besseli(1,t/2)*besselk(1,t/2)+besseli(2,t/2)* ...
        besselk(2,t/2)+0.5*t*(besseli(2,t/2)*besselk(1,t/2)- ...
        besseli(1,t/2)*besselk(2,t/2)))/San);
    d2Hds2 = imag(t^2*((8+t^2)*(besseli(1,t/2)*besselk(1,t/2)- ...
        besseli(2,t/2)*besselk(2,t/2))+t*(besseli(2,t/2)* ...
        besselk(1,t/2)-besseli(1,t/2)*besselk(2,t/2)))/(2*San)^2);
    ds = dHds * (imag(h)-ho) / ( dHds^2 + (imag(h)-ho)*d2Hds2 );
    San = s0 - ds;
    t = (1+1i)* r * sqrt(San*f/10) * 2e-3 * pi;
    h = t^2*(besseli(1,t/2)*besselk(1,t/2) - besseli(2,t/2)*besselk(2,t/2));
    fi = (imag(h)-ho)^2;
    cont2 = 0;
    while (fi>fi0)
        cont2 = cont2 + 1;
        San = s0 - ds/2;
        t = (1+1i)* r * sqrt(San*f/10) * 2e-3 * pi;
        h = t^2*(besseli(1,t/2)*besselk(1,t/2) - besseli(2,t/2)*besselk(2,t/2));
        fi = (imag(h)-ho)^2;
        if cont2 > 4
            break
        end
    end
    fi0 = fi;
    s0 = San;
    if cont1 > 9
        break
    end
end
San = San * 1000;

```

REFERENCES

- Andrade, F., T. Fischer, and J. Valenta, 2016, Study of errors in conductivity meters using the low induction number approximation and how to overcome them: Presented at the Conference Proceedings, Near Surface Geoscience 2016., European Association of Geoscientists & Engineers. doi: <https://doi.org/10.3997/2214-4609.201602080>.
- Beamish, D., 2011, Low induction number, ground conductivity meters: A correction procedure in the absence of magnetic effects: *Journal of Applied Geophysics*, **75**, 244–253, doi: <https://doi.org/10.1016/j.jappgeo.2011.07.005>.
- Freimann, B. C., J. G. das Virgens Alves, and M. W. C. Silva, 2014, Estudo hidrogeológico através de perfis geofísicos de poços – Salinópolis - PA: *Águas Subterrâneas*, **28**, 14–30.
- Guillemoteau, J., F.-X. Simon, E. Lück, and J. Tronicke, 2016, 1d sequential inversion of portable multi-configuration electromagnetic induction data: *Near Surface Geophysics*, **14**, 411–420, doi: [10.3997/1873-0604.2016029](https://doi.org/10.3997/1873-0604.2016029).
- Hanssens, D., S. Delefortrie, C. Bobe, T. Hermans, and P. De Smedt, 2019, Improving the reliability of soil ec-mapping: Robust apparent electrical conductivity (reca) estimation in ground-based frequency domain electromagnetics: *Geoderma*, **337**, 1155–1163, doi: <https://doi.org/10.1016/j.geoderma.2018.11.030>.
- He, X., H. Wang, and S. Ma, 2017, Translation algorithm of the apparent conductivity using the frequency-

- domain electromagnetic method of a magnetic dipole: *Journal of Applied Geophysics*, **146**, 221–227, doi: <https://doi.org/10.1016/j.jappgeo.2017.09.015>.
- Huang, H., and I. J. Won, 2000, Conductivity and susceptibility mapping using broadband electromagnetic sensors: *Journal of Environmental and Engineering Geophysics*, **5**, 31–41, doi: 10.4133/JEEG5.4.31.
- Jin, J.-M., 2015, *The finite element method in electromagnetics*, third ed.: Wiley.
- Kruk, J., J. Meekes, P. Van Den Berg, and J. Fokkema, 2000, An apparent-resistivity concept for low-frequency electromagnetic sounding techniques: *Geophysical Prospecting*, **48**, 1033 – 1052, doi: 10.1046/j.1365-2478.2000.00229.x.
- Li, Y., and K. Key, 2007, 2d marine controlled-source electromagnetic modeling: Part 1 — an adaptive finite-element algorithm: *GEOPHYSICS*, **72**, WA51–WA62, doi: 10.1190/1.2432262.
- McNeill, J. D., 1980, *Electromagnetic terrain conductivity measurements at low induction numbers*: Technical Note TN-6, Geonics Ltd.
- Méndez-Delgado, S., E. Gómez-Treviño, and M. A. Pérez-Flores, 1999, Forward modelling of direct current and low-frequency electromagnetic fields using integral equations: *Geophysical Journal International*, **137**, 336–352, doi: 10.1046/j.1365-246X.1999.00826.x.
- Rossetti, D., 2001, Late cenozoic sedimentary evolution in northeastern Pará, Brazil, within the context of sea level changes: *Journal of South American Earth Sciences*, **14**, 77–89, doi: 10.1016/S0895-9811(01)00008-6.
- Spies, B. R., and F. C. Frischknecht, 1987, *Electromagnetic sounding*, in *Electromagnetic Methods in Applied Geophysics*, Vol. 2, Application: SEG, volume 2 of *Investigations in Geophysics*, 285–425.
- Ward, S. H., and G. W. Hohmann, 1987, *Electromagnetic theory for geophysical applications*, in *Electromagnetic Methods in Applied Geophysics*, Vol. 1, Theory: SEG, volume 1 of *Investigations in Geophysics*, 130–311.

França E.T.: contributed to mathematical development, programming, coordination of field activities, data acquisition and processing, writing of the original manuscript, and revision; **Régis C.:** contributed to the supervision of the research, mathematical development, programming, contributed to the discussion of results, and revision of the text. **Cunha L.S.:** contributed to the characterization of the study area, identification of the problem/target applicable to the methodology, data acquisition and processing. **Françoso M.T.:** contributed to the bibliographic review, revision, and discussion of the text.